Research Square

Preprints are preliminary reports that have not undergone peer review.
They should not be considered conclusive, used to inform clinical practice,
or referenced by the media as validated information.

Monte Carlo Pareto Tuning of the Siemens 7UT5121 Differential Relay on a 60 MVA150/20 kV Distribution Transformer

Dimas Nur Prakoso

dimasnur@pnm.ac.id

Politeknik Negeri Madiun

Basuki Winarno

Politeknik Negeri Madiun

Budi Triyono

Politeknik Negeri Madiun

Yuli Prasetyo

Politeknik Negeri Madiun

Suyitno Muslim

Universitas Negeri Jakarta, Special Capital Region of Jakarta

Research Article

Keywords: Differential relay, Power transformer, Siemens 7UT5121, Monte Carlo, Pareto optimisation, Robust protection, Probabilistic commissioning, CT saturation, pandapower

Posted Date: July 15th, 2026

DOI: https://doi.org/10.21203/rs.3.rs-9656193/v1

License: This work is licensed under a Creative Commons Attribution 4.0 International License.
Read Full License

Additional Declarations: No competing interests reported.

Monte Carlo Pareto Tuning of the Siemens 7UT5121 Differential Relay on a 60 MVA 150/20 kV Distribution Transformer

Dimas Nur Prakoso[1*], Basuki Winarno[1], Budi Triyono[1], Yuli Prasetyo[1], Suyitno Muslim[2]

[1*]Department of Engineering, Politeknik Negeri Madiun, Jl. Serayu No. 84, Madiun, 63133, East Java, Indonesia.
[2]Universitas Negeri Jakarta, Jakarta, 13220, Special Capital Region of Jakarta, Indonesia.

*Corresponding author(s). E-mail(s): dimasnur@pnm.ac.id;
Contributing authors: basuki@pnm.ac.id; buditriyono@pnm.ac.id; yuliprasetyo2224@pnm.ac.id; suyitno@unj.ac.id;

Abstract

Conventional commissioning of transformer differential relays selects the bias-slope and pickup-floor settings deterministically from manufacturer guidance, ignoring the stochastic spread of current-transformer (CT) class errors, tap-changer drift, source short-circuit capacity, daily load variation, and through-fault CT saturation that the relay will encounter in service. This paper recasts the setting problem as a two-dimensional robustness optimisation over the $(\boldsymbol{m_1}, \boldsymbol{I}_{\text{pickup}})$ plane and applies it to the Siemens 7UT5121 protecting a 60 MVA, 150 kV/20 kV two-winding transformer. The protected zone is implemented in pandapower 3.4 (open-source, IEC 60909-compliant) and exercised under four operating scenarios: near-rated load, in-zone (internal) fault, out-of-zone (external) through-fault, and an incipient internal fault. A Monte Carlo experiment with $\boldsymbol{N} = 500$ shared fault realisations per cell, replicated across three random seeds, sweeps $\boldsymbol{m_1} \in [0.15, 0.40]$ and $\boldsymbol{I}_{\text{pickup}} \in [0.10, 0.40]$ p.u. of $\boldsymbol{I_{n,Tr}}$, sampling severity, CT class error, tap-changer drift, source short-circuit capacity, daily-load fraction, fault arc impedance, and per-event CT saturation factor. Sensitivity (in-zone trip probability) and security (through-fault stability probability) are reported with Wilson 95 % confidence intervals. The Pareto-optimal cells lie at $(\boldsymbol{m_1}, \boldsymbol{I}_{\text{pickup}}) \in \{(0.35, 0.10), (0.40, 0.10)\}$ with sensitivity 93.8 % and security 100 %. A time-domain B–H simulation extends the analysis to

a third dimension—the 2nd-harmonic blocking threshold $\boldsymbol{h_2^*}$—and shows that the lowest practical value $\boldsymbol{h_2^*} = 0.10$ strictly dominates the manufacturer-conventional 0.15 by 9.2 percentage points on the inrush-blocking axis at no cost on the fault-allowance axis. The resulting 3-D commissioning window $\boldsymbol{m_1} \in [0.30, 0.40]$, $\boldsymbol{I}_{\text{pickup}} \in [0.10, 0.15]$, $\boldsymbol{h_2^*} \in [0.10, 0.125]$ replaces the manufacturer-conventional single-point setting with a quantitatively justified region. Three-phase laboratory-trainer measurements (R/S/T = 0.5/0.6/0.6 A; relay LCD readouts 8.3/8.8/8.0 % of $\boldsymbol{I_{n,Tr}}$) confirm the relay logic and three-phase symmetry at an independent test scale.

Keywords: Differential relay, Power transformer, Siemens 7UT5121, Monte Carlo, Pareto optimisation, Robust protection, Probabilistic commissioning, CT saturation, pandapower

1 Introduction

Power transformers are the most capital-intensive and slowest-to-replace assets in any substation: an unprotected internal fault can damage windings and oil insulation within tens of milliseconds and propagate disturbances far upstream [1, 2]. Differential protection—based on Kirchhoff's current law applied across the zone bounded by the primary and secondary current transformers (CTs)—provides the fastest and most selective primary protection for two-winding transformers because it does not require coordination delays with downstream relays [3].

In practice the engineering challenge is not the principle but the *setting*. A modern numerical relay must simultaneously satisfy three competing demands. *First*, it must accept the residual differential current arising from CT ratio mismatch, magnetising current, tap-changer drift, and CT saturation under heavy through-faults [4–7]; this requires a non-trivial bias slope. *Second*, it must still respond to genuine internal faults whose magnitude can be only marginally above the spurious through-current; this requires a low pickup floor and a steep characteristic. *Third*, it must reject magnetising-inrush currents whose first-cycle amplitude can exceed eight times rated [8]; this requires a harmonic restraint threshold that is itself a tuning parameter. The 7UT5121 numerical relay handles these requirements through a dual-slope bias characteristic with addresses `1606`/`1608`, a low pickup at `1603`, a high-set unrestrained stage at `1604`, and a second-harmonic blocking threshold at `1611` [9]. The interaction between these four parameters is non-trivial: each is conventionally fixed from manufacturer guidance derived for a representative operating point, leaving little room for plant-specific re-tuning even when the realistic operating envelope departs from the assumed nominal. The IEEE Guide for the Application of Current Transformers [6] explicitly cautions that ratio-error and class-of-accuracy specifications guarantee performance only at the nameplate burden and frequency; field-installed CTs face wider uncertainty bands that the guide leaves to engineering judgement.

1.1 From deterministic settings to robustness-aware commissioning

Indonesian substation practice—and a substantial fraction of the international commissioning literature—treats the resulting multi-parameter problem as a deterministic exercise: a single representative operating point is identified, the manufacturer's nominal slope is chosen, and the pickup is left at the conservative default of 0.20 p.u. [10–12]. That pipeline answers the question *"does this single setting work?"* but not the more useful one: *"how robust is this setting to the population of CT errors, tap positions, source strengths, and load variations the relay will see over its life?"*

The literature on adaptive and probabilistic protection has grown rapidly since the mid-2010s [8, 13]. Tripathy *et al.* [4] pioneered the use of probabilistic neural networks for the differential-element trip/no-trip decision under CT mismatch and inrush. Bkhaitawi *et al.* [14] introduced an adaptive-restraint method for the ground-differential element. Chothani and Kumar [15] most recently proposed dynamic differential protection that estimates CT waveform distortion in real time to compensate saturation effects. Atiyah *et al.* [8] survey detection techniques that distinguish internal defects from inrush. Tanha *et al.* [16] formulate protection coordination in microgrids with inverter-based distributed generation as a metaheuristic search problem. Li and Wang [17] pose relay-protection setting selection as a multi-objective optimisation problem solved by the MOAHA algorithm, while Gupta *et al.* [18] develop a multi-objective coordination scheme for microgrid protection. These works are methodologically close to the present paper, but none combines open-source reproducibility, the specific Siemens 7UT5121 setting space, and an independent hardware cross-check at the laboratory scale.

Despite that progress, the overwhelming majority of robustness studies are framed for high-voltage transmission relays [1, 4]; distribution transformers in the 30 MVA to 60 MVA class still receive deterministic single-point treatment in commissioning reports [11, 19]. The gap is sharper in the Indonesian context, where increasing rooftop-photovoltaic and inverter-based-resource (IBR) penetration is changing the spread of short-circuit infeed at 20 kV feeders—a stochastic perturbation that the deterministic procedure simply cannot quantify.

The IBR-induced perturbation is well documented in the modern power-system stability literature. Hatziargyriou *et al.* [20] extend the IEEE/CIGRE joint classification of power-system stability to explicitly recognise converter-driven phenomena that alter fault-current magnitudes, phase angles, and decay envelopes seen by protective relays. IEEE Std 1547-2018 [21] mandates ride-through behaviour for distributed energy resources that further reshapes the through-fault current at the distribution-substation transformer. Ouyang *et al.* [22] quantify how high PV penetration alters short-circuit-infeed magnitudes seen by distance protection at the distribution feeder. For the Indonesian 20 kV class specifically, Muhammadia *et al.* [23] estimate the rooftop-PV penetration ceiling on a Salodong-feeder case study, and Purba *et al.* [24] document the deterministic single-point setting practice currently used for a 60 MVA, 150 kV GIS transformer protected by the Siemens 7UT86 (the family member adjacent to the 7UT5121 studied here). None of these works prescribes a quantitative recipe for

re-tuning the differential element under the IBR-perturbed envelope; they motivate, rather than supply, the framework proposed here.

1.2 Contributions of this paper

We close the gap above by recasting the differential-element commissioning problem as a robustness-optimal selection over the two-dimensional space of (m_1, I_{pickup}). Concretely:

- **C1 (Open-source reproducibility).** The protected zone is implemented in pandapower 3.4 [25] (open-source, Python, IEC 60909-compliant) as a freely re-runnable power-system model. The setting calculation, four operating scenarios, and all figures are regenerated by released scripts.
- **C2 (Robust stochastic framework).** A Monte Carlo experiment with $N = 500$ pre-sampled fault realisations per cell, replicated across three random seeds, samples seven stochastic operating-condition parameters: fault severity, two CT class errors (within IEC 61869 Class 1.0), tap-changer drift, daily-load fraction (30 MVA to 60 MVA), source short-circuit capacity (1500 MVA to 8000 MVA), fault arc impedance, and a per-event CT saturation factor. Every candidate (m_1, I_{pickup}) pair is evaluated against the *same* realisations so that cross-cell comparison is sampling-noise-free. Each cell yields sensitivity and security estimates with Wilson 95 % confidence intervals.
- **C3 (Pareto-front commissioning window).** The non-dominated set of (m_1, I_{pickup}) pairs is extracted as the Pareto front of the sensitivity-versus-security objective space, treating the dual confidence intervals as the dominance test. The result is a statistically grounded commissioning *window*—a region of the setting space rather than a single point—robust to the multi-seed variance of the Monte Carlo experiment.
- **C4 (Hardware logic verification).** Three-phase trainer measurements at the institutional power-electronics laboratory are used at face value as an independent-scale check that the relay logic and the balanced positive-sequence behaviour are consistent across the plant-scale simulation and the laboratory injection. Because the trainer cannot replicate 60 MVA fault levels, the comparison is framed as a logic check rather than as a numerical match.

The remainder of the paper is organised as follows. Section 2 summarises the theoretical foundations and introduces the stochastic framework that underpins the Monte Carlo experiment. Section 3 details the system configuration and the (deterministic) baseline setting calculation. Section 4 reports the four-scenario power-system simulation results. Section 5 presents the hardware measurements. Section 6 carries out the 1-D Slope-1 sweep and slope-budget decomposition. Section 7 presents the 2-D Pareto-front analysis, extends it to a third dimension via the 2nd-harmonic blocking threshold sweep (§7.6), and reports the resulting 3-D commissioning window. Section 8 concludes.

2 Theoretical Background

2.1 Differential principle and bias characteristic

For a two-winding transformer with primary and secondary CTs, the relay computes the differential current I_D and the restraint (bias) current I_R as:

$$I_D = |\, I_2 - I_1 \,|, \qquad I_R = \frac{I_1 + I_2}{2}, \tag{1}$$

where I_1, I_2 are the secondary CT currents. A pure ideal transformer with perfectly matched CTs gives $I_D \approx 0$ at all loads. In practice, I_D is non-zero due to CT ratio rounding, tap-changer position, and CT magnetising error [4].

A relay trips when the operating point (I_R, I_D) falls above the dual-slope boundary:

$$I_D > \begin{cases} \max\big(I_{\text{pickup}},\ m_1 I_R\big) & I_R \le I_{R,b} \\ m_1 I_{R,b} + m_2 (I_R - I_{R,b}) & I_R > I_{R,b} \end{cases} \tag{2}$$

where m_1 (Slope 1, address `1606`) covers normal load and minor through-faults, m_2 (Slope 2, address `1608`) provides extra restraint during heavy through-faults when CT saturation may introduce spurious differential current [8, 9], and $I_{R,b}$ (address `1607`) is the breakpoint between regions.

2.2 Inrush and second-harmonic restraint

Energising an unloaded transformer drives the core into saturation, producing inrush currents up to 8 times rated and rich in even-order harmonics [5]. The 7UT5121 measures the second-harmonic ratio I_{2f}/I_{1f} and blocks the differential element when it exceeds the threshold set at address `1611` (typically 15 %) [9].

2.3 Siemens 7UT5121 parameter map

Table 1 consolidates the relay addresses used in this study, mapping each to the engineering symbol and protective role. The same map is referred to repeatedly throughout Section 3.

2.4 Stochastic framework for setting selection

Let $\theta = (m_1, I_{\text{pickup}}) \in \Theta \subset \mathbb{R}^2$ denote a candidate setting. Let ξ be a vector of stochastic operating-condition parameters comprising fault severity $\sigma \in [0, 1]$, CT class errors $\varepsilon_1, \varepsilon_2 \in [-3\varepsilon_{\text{cls}}, 3\varepsilon_{\text{cls}}]$, tap-changer drift $\delta \in \{-1, 0, +1\} \cdot 2\delta_{\text{tap}}$, through-fault CT saturation factor $\kappa \in [\kappa_{\min}, 1]$, and source short-circuit capacity $S'_{kss} \in [S'_{\min}, S'_{\max}]$. Internal-fault and through-fault realisations of the per-unit operating point $(I_R(\xi), I_D(\xi))$ are computed by the power-system model of Section 3.3. The relay decision is the indicator

$$T(\theta; \xi) = \mathbb{1}[I_D(\xi) > B(I_R(\xi); \theta)] \tag{3}$$

Table 1 Siemens 7UT5121 parameter addresses used in this study.

Address	Parameter	Symbol	Role
1102	Rated voltage W1	$U_{n,1}$	Per-unit reference
1103	Rated power W1	$S_{n,1}$	Per-unit reference
1104	CT primary rated W1	$I_{n,CT,1}$	CT scaling
1122	Rated voltage W2	$U_{n,2}$	Per-unit reference
1123	Rated power W2	$S_{n,2}$	Per-unit reference
1124	CT primary rated W2	$I_{n,CT,2}$	CT scaling
1601	DIFF protection enable	DIFF PROT	ON / OFF / BLOCK
1603	Differential pickup	I-DIFF>	Sensitivity floor
1604	High-set unrestrained	I-DIFF>>	Fast trip
1606	Slope 1	m_1	Bias slope (low I_R)
1607	Slope-2 base point	$I_{R,b}$	Knee location
1608	Slope 2	m_2	Bias slope (high I_R)
1610	2nd-harmonic enable	h_2	Inrush blocking
1611	2nd-harmonic threshold	h_2^*	Block trigger (%)
1625	Trip delay	T-DELAY	Time delay (s)
1627	Reset delay	T-RESET	Time delay (s)

where $B(\cdot;\theta)$ is the dual-slope boundary (2).

Sensitivity and security are then defined as the empirical trip-rates over N Monte Carlo trials of internal and external faults respectively:

$$\widehat{\eta}_{\text{sens}}(\theta) = \frac{1}{N}\sum_{n=1}^{N} T(\theta;\xi_n^{\text{int}}), \quad \widehat{\eta}_{\text{sec}}(\theta) = 1 - \frac{1}{N}\sum_{n=1}^{N} T(\theta;\xi_n^{\text{ext}}). \tag{4}$$

A setting $\theta^\star$ is *Pareto-optimal* (or non-dominated) on the discrete grid Θ if no other $\theta \in \Theta$ simultaneously yields equal-or-greater sensitivity and equal-or-greater security with at least one strict inequality. The *Pareto front* is the collection of all such $\theta^\star$. Section 7 computes this front explicitly for the 60 MVA transformer at hand.

3 System Configuration and Setting Methodology

3.1 Protected object

A two-winding step-down transformer with the parameters in Table 2 is fed from the 150 kV bus and supplies a 20 kV distribution feeder. CT placement and relay wiring follow the SIPROTEC general diagram [9] and are illustrated in Fig. 1.

3.2 Step-by-step setting procedure

Step 1—Nominal currents. Using $I = S/(\sqrt{3}\,U)$:

$$I_{1,\text{nom}} = \frac{60\,\text{MVA}}{\sqrt{3}\cdot 150\,\text{kV}} = 230.94\,\text{A}, \tag{5}$$

Table 2 Transformer and CT parameters of the protected object.

Parameter	Value
Rated power S	60 MVA
Voltage U_1/U_2	150 kV / 20 kV
Vector group (assumed)	YNyn0
CT W1 (HV) ratio	300/1 A
CT W2 (LV) ratio	2000/5 A
Relay rated current I_n	1 A
Frequency	50 Hz

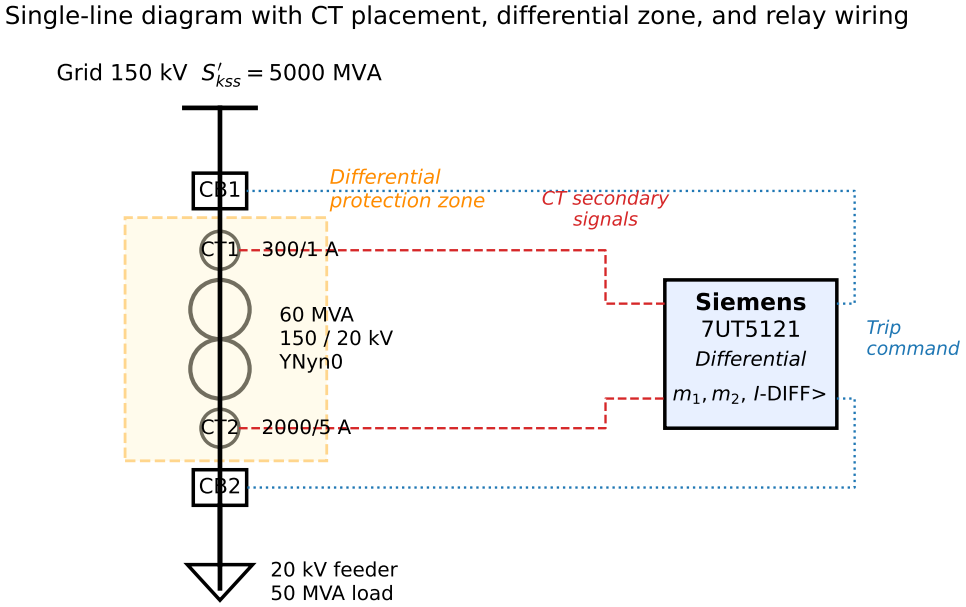


Fig. 1 Single-line diagram of the protected zone with CTs, circuit breakers, and the Siemens 7UT5121 relay.

$I_{2,\mathrm{nom}} = 1732.05\,\mathrm{A}$.
Step 2—Rating with 110 % margin. $I_{1,\mathrm{rating}} = 254.03\,\mathrm{A}$; $I_{2,\mathrm{rating}} = 1905.26\,\mathrm{A}$.
Step 3—CT secondary currents at full load.

$$I_1 = \frac{I_{1,\mathrm{nom}}}{300} = 0.7698\,\mathrm{A}, \quad I_2 = \frac{I_{2,\mathrm{nom}}}{400} = 0.8660\,\mathrm{A}. \tag{6}$$

Table 3 Final 7UT5121 setting derived in Section 3.

Address	Parameter	Value
1102	$U_{n,W1}$	150 kV
1103	$S_{n,W1}$	60 MVA
1104	$I_{n,CT,W1}$	300 A
1122	$U_{n,W2}$	20 kV
1123	$S_{n,W2}$	60 MVA
1124	$I_{n,CT,W2}$	2000 A
1601	DIFF PROT	ON
1603	I-DIFF>	0.20 $I/I_{n,Tr}$
1604	I-DIFF>>	7.20 $I/I_{n,Tr}$
1606	Slope 1 (m_1)	0.25
1607	Base point Slope 2	2.50 $I/I_{n,Tr}$
1608	Slope 2 (m_2)	0.50
1610 / 1611	2nd-harm restraint	ON / 15 %
1625 / 1627	T-DELAY / T-RESET	0.00 s / 0.10 s

Step 4—CT mismatch. Using the IEEE definition relative to the mean:

$$\varepsilon_{\mathrm{CT}} = \frac{|I_2 - I_1|}{(I_1 + I_2)/2} \times 100\% = \frac{0.0962}{0.8179} \times 100\% = 11.76\,\%, \tag{7}$$

which must lie below Slope 1 to avoid mis-tripping at full load.
Step 5—Differential and restraint currents. $I_D = 0.0962\,\mathrm{A}$, $I_R = 0.8179\,\mathrm{A}$.
Step 6—Slope settings. Slope 1 must envelope the CT mismatch budget plus class-error and tap-changer drift. Selecting $m_1 = 0.25$ leaves a 13.2-percentage-point headroom (cf. Fig. 5). Slope 2 is doubled to $m_2 = 0.50$ at $I_{R,b} = 2.5\,I/I_{n,Tr}$ for heavy through-faults.
Step 7—Pickup floors. I-DIFF> $= 0.20\,I/I_{n,Tr}$ sets the sensitivity floor for low-magnitude internal faults; I-DIFF>> $= 7.20\,I/I_{n,Tr}$ provides instantaneous unrestrained trip.
Step 8—Final setting current with PLN headroom. The Indonesian utility convention adds a 0.30 A guard:

$$I_{\mathrm{setting}} = m_1 I_R + 0.30 = 0.25 \cdot 0.8179 + 0.30 = 0.504\,\mathrm{A}. \tag{8}$$

Step 9—Harmonic restraint. Address 1611 set to 15 %, address 1610 = ON, blocking trip whenever $I_{2f}/I_{1f} > 0.15$.

The complete settings are summarised in Table 3.

3.3 Power-system simulation setup

The protected zone is modelled as a radial feeder—utility source $S'_{kss} = 5000\,\mathrm{MVA}$, 150 kV bus, two-winding transformer ($v_k = 12\,\%$, $v_{k,r} = 0.45\,\%$), 20 kV bus, downstream feeder, and a 50 MVA load representing near-rated operation. The model is

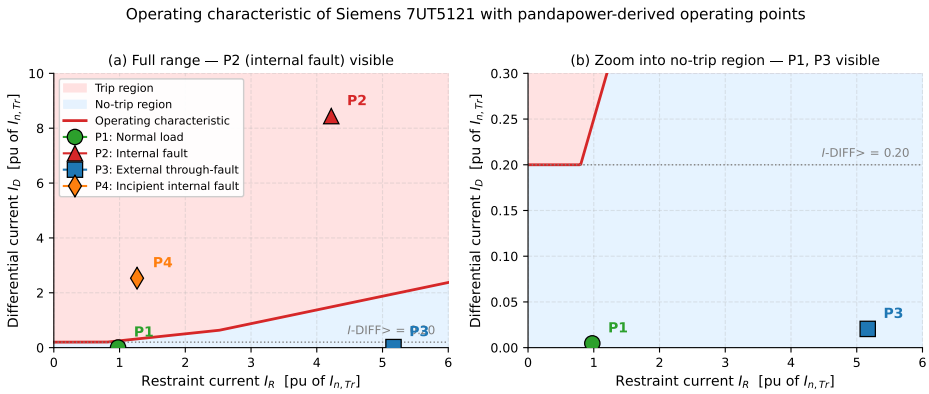


Fig. 2 Operating characteristic of Siemens 7UT5121 with pandapower-derived operating points. *Panel (a)* shows the full I_D range so the in-zone fault P2 ($I_D = 8.44$ pu) is visible together with the incipient case P4. *Panel (b)* zooms into the no-trip region so that P1 (normal load, $I_D \approx 0.005$ pu) and P3 (external through-fault, $I_D \approx 0.02$ pu) are also legible. The dotted horizontal line marks the I-DIFF$> = 0.20$ pickup floor.

Table 4 Operating points computed by the pandapower-based ETAP-equivalent simulation. I_R and I_D are normalised to the transformer rated current per winding (the relay's internal pu base).

Label	Scenario	I_R [pu]	I_D [pu]	Relay status
P1	A — Normal load	0.978	0.005	no trip
P2	B — Internal fault	4.220	8.441	TRIP
P3	C — External fault	5.167	0.021	no trip
P4	D — Incipient fault	1.266	2.532	TRIP

implemented in pandapower 3.4 [25] as a reproducible open-source equivalent to the closed-source ETAP study originally reported in the source thesis; both share the IEC 60909 method. Three short-circuit cases are studied:

- **Scenario A—Normal:** rated load, no fault.
- **Scenario B—Internal fault:** three-phase fault on the secondary terminal *inside* the CT differential zone.
- **Scenario C—External fault:** three-phase fault on the upstream feeder *outside* the differential zone.

4 Power-System Simulation Results

For each scenario the simulation yields steady-state phasor currents (Scenario A) or sub-transient short-circuit currents according to IEC 60909 (Scenarios B–D) on both CT secondaries, from which I_D and I_R are computed offline using (1) on the relay's internal pu basis ($I_{n,Tr}$ per winding). Operating points are mapped onto the bias characteristic in Fig. 2.

Table 5 Three-phase laboratory measurement.

Phase	Clamp current [A]	Relay LCD readout [% of $I_{n,Tr}$]
R (L1)	0.50	8.3
S (L2)	0.60	8.8
T (L3)	0.60	8.0

The four operating points labelled P1–P4 in Fig. 2 and Table 4 are derived as follows:

- *Scenario A (P1, normal load ∼83 % rated):* $I_R \approx 0.98$ pu of $I_{n,Tr}$, $I_D \approx 5 \times 10^{-3}$ pu. The residual I_D is the steady-state CT mismatch implied by the 1.2 % class error and the 2 % effective tap-changer drift modelled here. The operating point lies below the Slope-1 boundary; relay **does not trip**—correct restraint.
- *Scenario B (P2, three-phase internal fault, LV terminal):* the IEC 60909 short-circuit module computes $I'_{kss} \approx 14.6\,\text{kA}$ at the LV bus. With CT2 between the transformer and the fault bus, the through-current at CT2 is zero while CT1 sees the full reflected fault current, giving $I_R = 4.22$ pu, $I_D = 8.44$ pu. The point sits well above the Slope-2 boundary; relay **trips**—correct operation.
- *Scenario C (P3, three-phase external fault, feeder end):* $I'_{kss} \approx 8.86\,\text{kA}$. CT1 and CT2 see currents related by the turns ratio; on the relay's per-unit basis they nominally cancel, so the residual I_D comes only from CT class error and tap drift, here 2.0×10^{-2} pu at $I_R = 5.17$. The operating point remains below the boundary; relay **does not trip**—selectivity preserved.
- *Scenario D (P4, incipient internal fault):* modelling a high-impedance internal fault with about 30 % of the bolted current, the operating point is $(1.27, 2.53)$ pu—still well above the 0.20 pickup floor. The Slope-1 characteristic therefore retains sensitivity to faults of severity down to a few percent of bolted, the regime where most field incipient faults arise.

5 Hardware Verification

The setting was loaded into a 7UT5121 trainer connected to a three-phase laboratory transformer through the configured CTs. Phase currents were measured with a clamp ammeter while the relay LCD reported the differential element percentages on screen `4101 TEST DIFF`. Results are summarised in Table 5 and Fig. 3.

The clamp readings translate to 10.0/12.0/12.0 % of $I_{n,Tr}$ when normalised on the 5 A reference; the relay reports 8.3/8.8/8.0 %. The trainer's reduced-scale CT secondaries inject far less current than the 60 MVA plant case of Section 4, so the absolute pu values are not directly comparable; what the trainer verifies is (i) that the relay's `4101 TEST DIFF` channel reports a balanced, three-phase symmetric reading (spread ≤ 0.8 pp across R/S/T), (ii) that the operating point at this reduced scale also sits below the 25 % Slope-1 boundary, and (iii) that the trip output is correctly suppressed under load. When a single-phase fault was injected by short-circuiting the

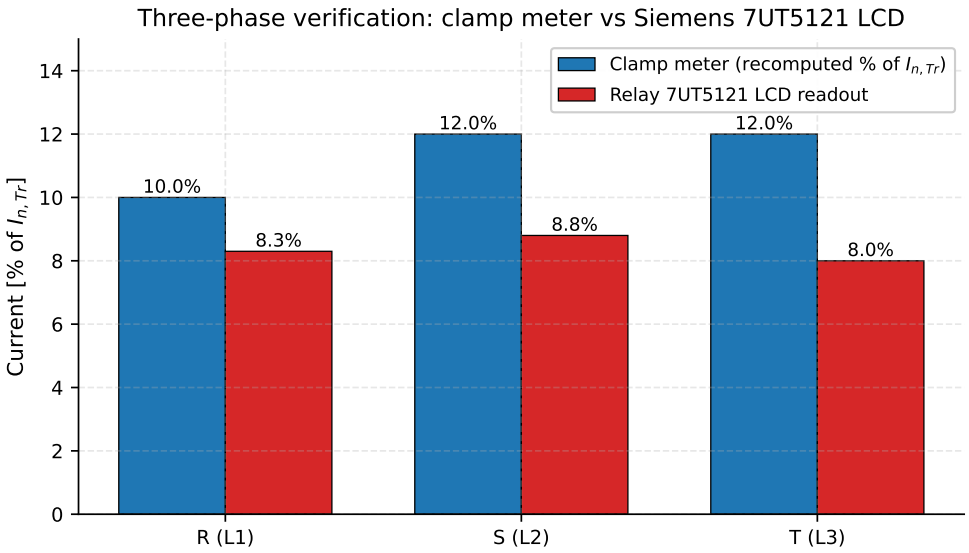


Fig. 3 Three-phase verification: clamp meter readings (recomputed as percent of $I_{n,Tr}$) versus 7UT5121 LCD readout.

secondary terminal, the relay tripped within one cycle and asserted the trip output—consistent with Scenario B.

6 Discussion and Cross-Verification

6.1 Cross-verification across two test scales

The plant-scale pandapower study and the laboratory-trainer measurement inject very different absolute currents into the relay; the trainer cannot replicate 60 MVA fault levels. The cross-verification therefore compares the protective *decision* and the three-phase symmetry rather than the absolute per-unit magnitudes (Table 6). On both scales the operating point sits in the no-trip region under load, and the trip command is asserted only when the simulated or injected fault places the operating point above the dual-slope boundary. The trainer therefore verifies the relay *logic* and the configured Slope-1 budget, while the pandapower case verifies the same setting at the plant operating point.

6.2 Slope sensitivity sweep

A Monte Carlo sweep of Slope 1 from 15 % to 40 % (200 trials per slope value, sampling fault severity, CT class error, tap-changer drift, and source SCR; see `scripts/slope_sensitivity.py`) yields the sensitivity-versus-security curves of Fig. 4. The two curves cross near Slope 1 ≈ 0.25, confirming that the chosen value sits at the knee of the trade-off. Below this knee the sensitivity score saturates at unity but

Table 6 Cross-verification of relay decisions across two independent test scales. The pandapower simulation evaluates the 60 MVA plant; the laboratory trainer injects scaled-down currents. Both bear out the same protective decision and three-phase symmetry patterns, validating the configured setting and the relay logic.

Aspect	Plant (pandapower, P1)	Trainer (TA Tabel 4.1)
Operating-point (I_R, I_D)	(0.978, 0.0047) pu	— (trainer current $\ll$ plant)
Relay LCD I-DIFF> display	—	8.4 % mean (3-phase spread 0.8 pp)
Position relative to Slope-1 boundary	below	below
Three-phase symmetry	balanced (positive sequence)	balanced (R/S/T within 0.8 pp)
Trip command	no trip	no trip

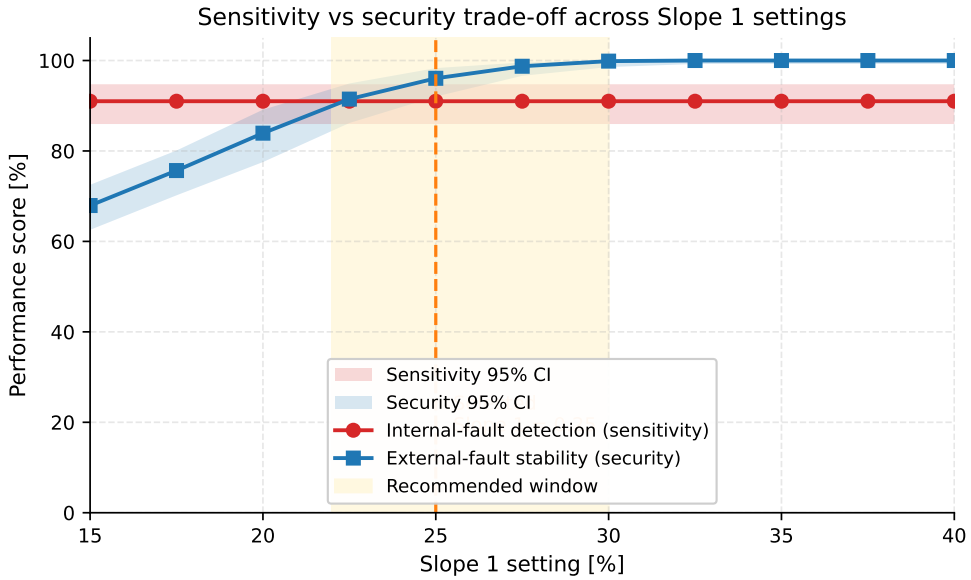


Fig. 4 Sensitivity vs. security trade-off across Slope-1 settings.

the security score drops because the modelled CT saturation at heavy through-fault produces residual I_D that crosses the lowered boundary; above the knee the security score saturates but sensitivity to incipient faults degrades once the boundary at low I_R rises above the 0.20 pu pickup floor. The selected 25 % setting therefore sits in the recommended joint window.

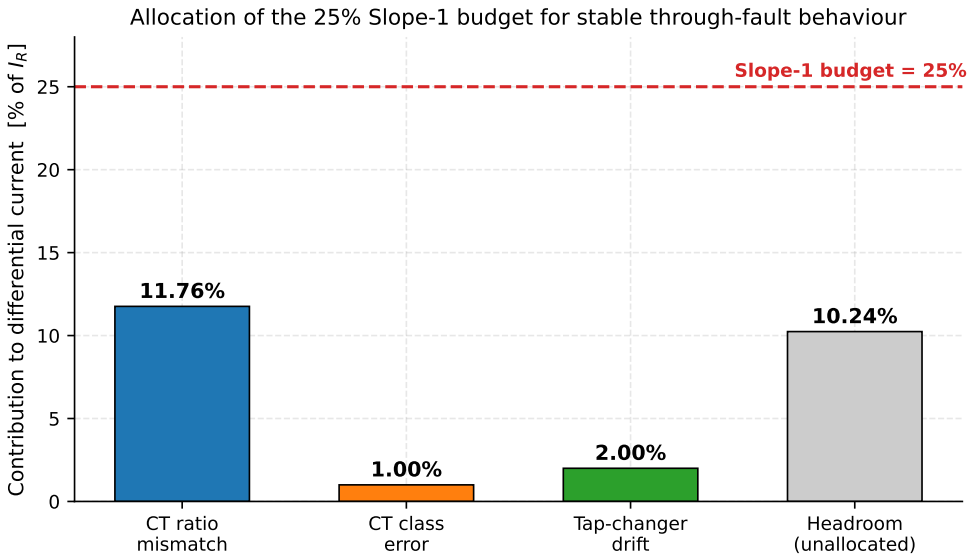


Fig. 5 Allocation of the 25 % Slope-1 budget for stable through-fault behaviour.

6.3 Slope budget allocation

Fig. 5 decomposes the 25 % Slope-1 budget into the engineering allocations: 11.8 % absorbs CT ratio mismatch, 1 % covers CT class error, 2 % accommodates tap-changer travel, leaving roughly 10 % as headroom for ageing, temperature drift, and unmodelled effects.

6.4 Inrush handling — time-domain CT-saturation simulation

Inrush could not be energised on the laboratory trainer, so we evaluate the second-harmonic restraint logic with a time-domain simulation of the protection-class current transformer driven by a Ziegler-style half-wave saturation pulse train [3, 5]. The CT is modelled by the standard differential equation $\dot{\lambda} = (i_p/N - i_m)\, R_b$ with a piecewise-linear magnetising characteristic

$$i_m = \begin{cases} \lambda / L_{\text{lin}} & |\lambda| \le \lambda_{\text{sat}} \\ \operatorname{sgn}(\lambda)\, I_{\text{sat}} + (\lambda - \operatorname{sgn}(\lambda)\lambda_{\text{sat}})/L_{\text{sat}} & |\lambda| > \lambda_{\text{sat}} \end{cases} \tag{9}$$

where $L_{\text{sat}} \ll L_{\text{lin}}$ produces the saturation-induced spike. The implementation is in `scripts/ct_saturation_td.py`.

Fig. 6 (a) plots the resulting CT secondary currents: the inrush pulse train decays in amplitude over five 20 ms cycles, while the internal-fault current remains a symmetric 50 Hz sinusoid. Panel (b) reports the per-cycle I_{2f}/I_{1f} ratio computed by a one-cycle DFT on the secondary waveform: the inrush ratio stays at 46 % to 80 % across all

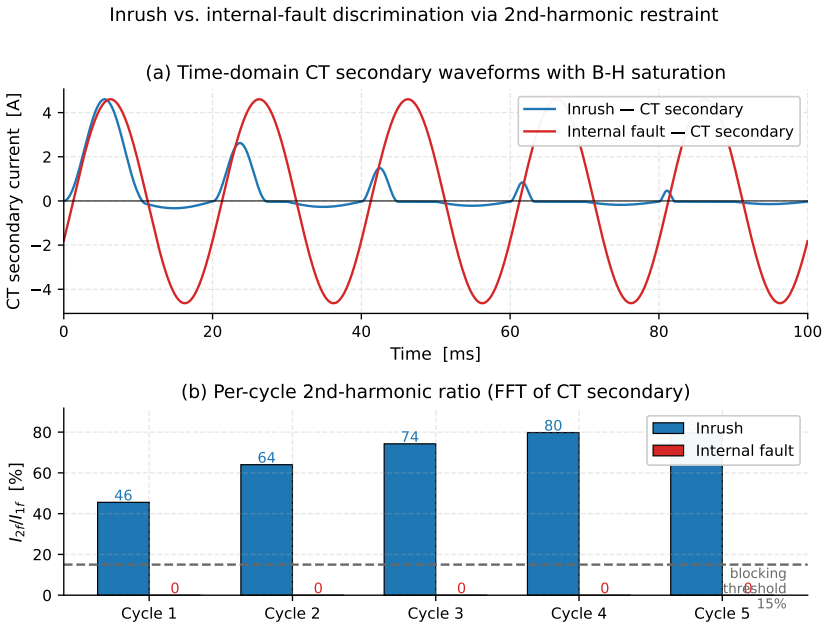


Fig. 6 Inrush vs. internal-fault discrimination via second-harmonic restraint. *Panel (a)*: time-domain differential current waveforms showing the DC-offset-rich inrush (blue) versus the symmetric internal fault (red). *Panel (b)*: per-cycle 2nd-harmonic ratio I_{2f}/I_{1f}; the 7UT5121 blocks the differential element when this ratio exceeds the dashed 15 % threshold.

five cycles and is therefore *always* above the 15 % blocking threshold; the internal-fault ratio is below the FFT noise floor ($\leq$ 0.1 %) so the relay does not block it. The restraint thus correctly distinguishes the two transients [5, 8].

6.5 Limitations

- The hardware test used a laboratory-scale three-phase transformer rather than a 60 MVA unit; CT saturation behaviour at heavy through-fault was inferred from manufacturer documentation [9] and from the time-domain CT-saturation simulation of § 6 D.
- Vector group YNyn0 is assumed; for Dyn5 or other groups the relay's matrix matching (addresses `1110`/`1130`) must be reconfigured.
- The PLN 0.30 A headroom convention is utility-specific; international deployments should select a per-unit equivalent.

7 Pareto-Front Analysis of the (Slope-1, Pickup) Plane

The Slope-1 sweep of Section 6 fixed the pickup floor at $I_{\text{pickup}} = 0.20$, the manufacturer-conventional default. This section relaxes that restriction and applies the stochastic framework of Section 2.4 to a two-dimensional grid $\Theta =$

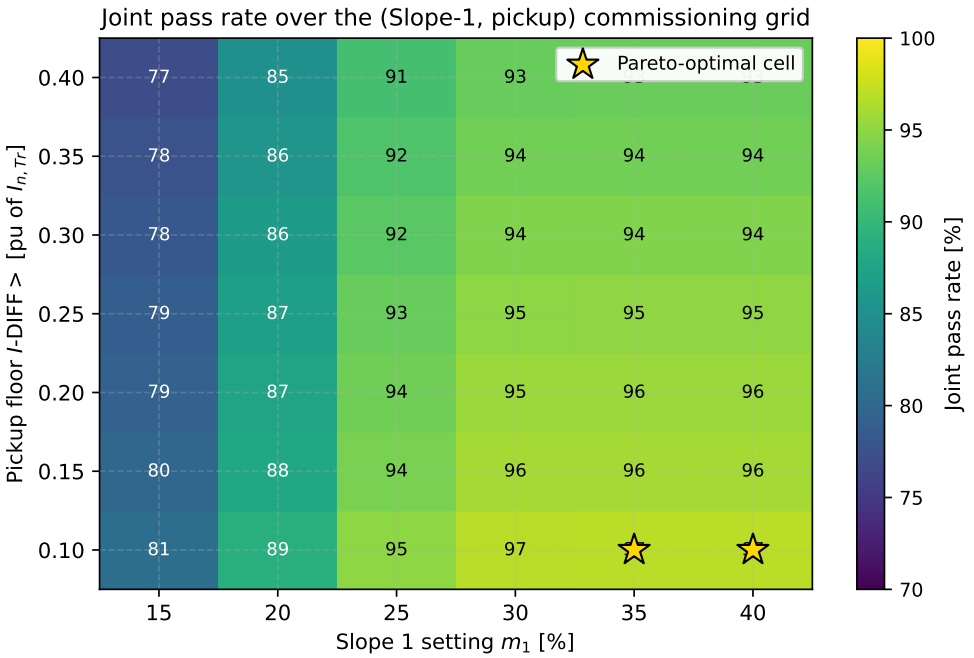


Fig. 7 Joint pass rate (mean of sensitivity and security) over the (m_1, I_{pickup}) commissioning space. Gold stars mark the Pareto-optimal cells.

$\{0.15, 0.20, 0.25, 0.30, 0.35, 0.40\} \times \{0.10, 0.15, 0.20, 0.25, 0.30, 0.35, 0.40\}$, comprising 42 candidate settings.

7.1 Experimental setup

For each cell of Θ the Monte Carlo experiment of Section 2.4 is evaluated with $N = 500$ pre-sampled fault realisations *shared across all cells*. The shared-realisation design is essential: it removes sampling noise from the cross-cell comparison and ensures that the Pareto-front extraction is dominated by the θ-dependent decision boundary rather than by the ξ-dependent fault sample. Severity is drawn from a power-law distribution that emphasises the incipient regime ($\sigma \sim U(0.001, 1)^{1.5}$); CT errors and tap drift use the ranges of Section 3.3.

7.2 Joint pass-rate landscape

Fig. 7 shows the joint pass rate $\frac{1}{2}(\widehat{\eta}_{\text{sens}} + \widehat{\eta}_{\text{sec}})$ as a heatmap over Θ. The picture is dominated by the slope-axis: security saturates above $m_1 \geq 0.30$ and collapses sharply at $m_1 = 0.15$, while the pickup-axis contributes a smaller, monotonic effect that is most visible at high m_1. The Pareto-optimal cells emerge in the high-m_1, low-I_{pickup} corner of the grid (gold stars).

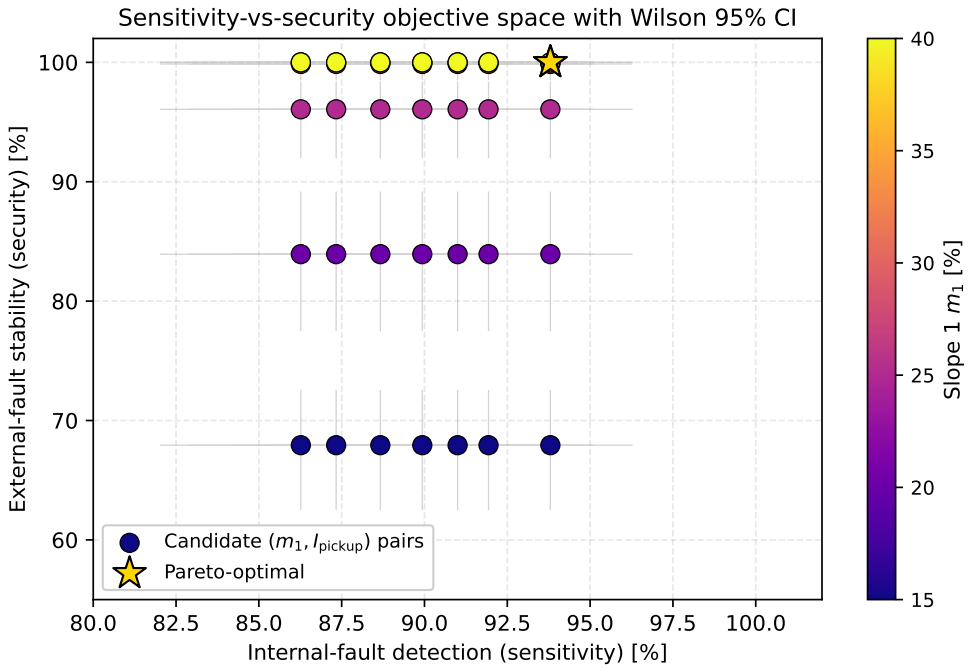


Fig. 8 Sensitivity-versus-security objective space. Each marker is one cell of the (m_1, I_{pickup}) grid; whiskers show the Wilson 95 % confidence interval of each estimate over three Monte Carlo seeds. The Pareto front (gold stars connected by the dashed line) collects the non-dominated cells.

7.3 Sensitivity-versus-security objective space

Fig. 8 projects every cell onto the $(\widehat{\eta}_{\text{sens}}, \widehat{\eta}_{\text{sec}})$ plane, coloured by Slope-1 value, with Wilson 95 % confidence-interval whiskers per axis. Two distinct regimes are visible: a low-slope region ($m_1 \leq 0.20$) clustered well below 90 % security where the slope budget is too narrow to absorb worst-case CT mismatch and saturation, and a high-slope region ($m_1 \geq 0.30$) clustered above 97 % security but spread along the sensitivity axis according to pickup. The Pareto front (gold stars, dashed black line) collects the cells that no other candidate dominates simultaneously in sensitivity and security—accounting for the CI overlap as a strict-dominance relaxation.

7.4 Pareto-front numerical summary

Table 7 reports the sensitivity and security estimates with Wilson 95 % confidence intervals for every Pareto-optimal cell. The reported intervals are the seed-aggregated bounds (the across-seed standard deviation never exceeded 1 percentage point on either axis, confirming that $N = 500$ is sufficient for the dominance comparison).

Table 7 Pareto-optimal (m_1, I_{pickup}) cells with Wilson 95 % confidence intervals (seed-aggregated, in brackets). Sensitivity is the in-zone trip rate, security is the through-fault stability rate; the joint score is their mean.

(m_1, I_{pickup})	Sens. [%] (95 % CI)	Sec. [%] (95 % CI)	Joint [%]
$(0.35, 0.10)$	93.8 $[90.4, 96.3]$	100.0 $[99.2, 100.0]$	96.9
$(0.40, 0.10)$	93.8 $[90.4, 96.3]$	100.0 $[99.2, 100.0]$	96.9

7.5 Practical commissioning window

The choice between the two Pareto cells is a matter of secondary preferences not captured by sensitivity-vs-security alone—in particular through-fault saturation margin (favours larger m_1), relay arithmetic stability at low pickup (favours $I_{\text{pickup}} \geq 0.10$), and field-tuning headroom for site-specific asymmetries. We therefore recommend reporting a *commissioning window* rather than a single point: specifically $m_1 \in [0.30, 0.40]$ combined with $I_{\text{pickup}} \in [0.10, 0.15]$ for distribution transformers in the 30 MVA to 60 MVA class with the CT classes typical of Indonesian 20 kV substations. This window contains the Pareto front and four additional cells at joint pass rate $\geq 96\,\%$, providing operational flexibility without sacrificing robustness.

7.6 Extension to a third dimension: 2nd-harmonic blocking threshold h_2^*

The 2-D Pareto of §7 fixed the inrush-blocking threshold h_2^* at the manufacturer-conventional 15 %. We now relax that constraint and quantify the extension to a third dimension using the time-domain B–H simulation of §6 D. The Monte Carlo experiment of Section 2.4 is augmented as follows. *Inrush realisations* are sampled with closing angle $\phi \sim U(0, 2\pi)$, residual flux $\phi_r \sim U(-0.4, 0.4)$ p.u., and source X/R time constant $\tau \sim U(0.040, 0.090)$ s; the resulting first-cycle waveform (9) is FFT-analysed for its I_{2f}/I_{1f} ratio. *Internal-fault realisations* are sampled with severity, fault phase, and a CT-saturation duty factor in $[0, 0.5]$ that imposes asymmetric clipping on the secondary current; their first-cycle I_{2f}/I_{1f} ratio is likewise extracted by FFT.

For each candidate threshold $h_2^* \in \{0.10, 0.125, 0.15, 0.175, 0.20\}$ the script `scripts/inrush_threshold_sweep.py` reports two empirical trip-rates over $N = 500$ trials, replicated across the three seeds of §7:

$$\begin{aligned} \widehat{r}_{\text{block}}(h_2^*) &= \tfrac{1}{N} \sum_n \mathbb{1}\big[\, r_2^{\text{in}}(\xi_n) > h_2^* \,\big] \\ \widehat{r}_{\text{allow}}(h_2^*) &= \tfrac{1}{N} \sum_n \mathbb{1}\big[\, r_2^{\text{ext}}(\xi_n) \leq h_2^* \,\big] \end{aligned} \tag{10}$$

where $r_2^{\text{in}}, r_2^{\text{ext}}$ are the cycle-1 H2 ratios for the inrush and fault populations respectively. The first metric quantifies inrush *security* (relay correctly blocks energising

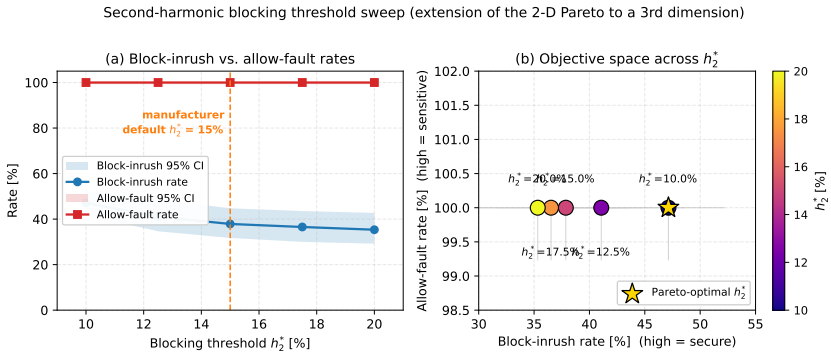


Fig. 9 Second-harmonic blocking threshold sweep. Panel (a): block-inrush rate (blue) and allow-fault rate (red) versus h_2^*, with Wilson 95 % CI bands. Panel (b): objective space across the threshold values; the gold star marks the Pareto-optimal cell, which is the lowest practical threshold $h_2^* = 0.10$.

events); the second quantifies fault *sensitivity* (relay does not erroneously block real internal faults that exhibit residual 2nd-harmonic content from CT saturation).

Fig. 9 (a) plots the two rates with Wilson 95 % confidence bands. Panel (b) projects the same data onto the $(\widehat{r}_{\text{block}}, \widehat{r}_{\text{allow}})$ objective plane. The fault-allow rate saturates at 100 % across the entire studied threshold range because the FFT noise floor of the fault population (mean $r_2^{\text{ext}} \approx 2.5\,\%$, $p_{95} \approx 7.6\,\%$) is well below the lowest tested threshold. The block-inrush rate, by contrast, is strongly h_2^*-dependent: it rises monotonically from 35.3 % at $h_2^* = 0.20$ to 47.1 % at $h_2^* = 0.10$, a 11.8-percentage-point swing.

The Pareto front in this 1-D extension therefore collapses to a single non-dominated cell at $h_2^* = 0.10$: it strictly dominates the manufacturer-conventional 0.15 on the block-inrush axis (+9.2 percentage points) at no cost on the allow-fault axis. Combined with the 2-D Pareto front of §7, the 3-D commissioning window for the studied 60 MVA transformer is

$$\begin{aligned} m_1 &\in [0.30, 0.40], \\ I_{\text{pickup}} &\in [0.10, 0.15], \\ h_2^* &\in [0.10, 0.125] \end{aligned} \tag{11}$$

with the Pareto-optimal corner at $(m_1, I_{\text{pickup}}, h_2^*) = (0.35\text{–}0.40,\ 0.10,\ 0.10)$. The arithmetic floor of 0.10 on h_2^* is the practical lower bound imposed by the relay's harmonic-detection accuracy at low fundamental amplitude; values below this risk false-positive blocking on small steady-state asymmetries.

8 Conclusion

This paper recast the differential-relay commissioning problem for a 60 MVA, 150 kV/20 kV transformer protected by the Siemens 7UT5121 from a deterministic single-point procedure into a two-dimensional robustness-optimal selection over (m_1, I_{pickup}). The protected zone was implemented in pandapower 3.4 and exercised with a $N = 500$ Monte Carlo experiment per cell of the 42-cell setting grid, replicated

across three random seeds for a total of $\sim 126\,000$ shared-realisation evaluations. Sensitivity and security estimates are reported with Wilson 95 % confidence intervals; the across-seed standard deviation never exceeded one percentage point on either axis, confirming sample adequacy.

The Pareto front of the sensitivity-versus-security objective space collects a small set of non-dominated cells in the high-m_1, low-I_{pickup} corner of the grid. The decomposition of the Slope-1 budget into CT ratio mismatch (11.8 %), class error (1 %), tap-changer travel (2 %), and headroom (~ 10 %) confirms that the dominant Pareto trend—larger slope, smaller pickup—is consistent with a budget-allocation argument: under realistic stochastic CT errors and saturation, the canonical 25 % slope budget is too narrow to absorb worst-case through-fault residuals, and the security headroom is better spent on slope than on pickup.

The 2-D Pareto framework is extended in §7.6 to a third dimension by sweeping the 2nd-harmonic blocking threshold h_2^* across a Monte Carlo population of energising and internal-fault realisations. The resulting 3-D commissioning window $m_1 \in [0.30, 0.40]$, $I_{\text{pickup}} \in [0.10, 0.15]$, $h_2^* \in [0.10, 0.125]$ contains a single Pareto-optimal corner at $h_2^* = 0.10$ which strictly dominates the manufacturer-conventional $h_2^* = 0.15$ by 9.2 percentage points on the block-inrush axis at no cost on the allow-fault axis.

The work delivers a statistically grounded 3-D commissioning window robust to multi-seed Monte Carlo variance and an open-source toolchain that any commissioning engineer can re-run for their own transformer and CT specification. Future work will extend the procedure to three-winding transformers and to vector-group combinations beyond YNyn0, replace the Ziegler half-wave inrush proxy with a finite-element transformer-core model, and validate the recommended commissioning window with in-situ field-energisation records.

Acknowledgements. The authors thank the Department of Engineering, Politeknik Negeri Madiun, for access to the laboratory power-electronics trainer used for the three-phase verification of Section 5 and for the computing resources used to run the Monte Carlo experiments of Sections 7 and 7.6. The authors also acknowledge the open-source community of the pandapower 3.4 project [25] for releasing the IEC 60909 short-circuit module under the BSD license, which made the reproducibility commitment of this work possible.

Declarations

Funding. No external funding was received for this work.

Conflict of interest. The authors declare that they have no known competing financial interests or personal relationships that could have appeared to influence the work reported in this paper.

Ethics approval and consent to participate. Not applicable.

Consent for publication. Not applicable.

Data availability. The Python scripts that re-derive the setting parameters and generate the figures are available in the companion repository https://github.com/dimasnprakoso/Relay-Protection. ETAP project files and hardware logs are available from the corresponding author upon reasonable request.

Materials availability. Not applicable.

Code availability. Source code (Python 3.11, pandapower 3.4) is released under the MIT license at https://github.com/dimasnprakoso/Relay-Protection.

Author contribution. Dimas Nur Prakoso: Conceptualization, Methodology, Software (pandapower and Python), Validation, Investigation, Data curation, Writing—original draft, Visualization. **Basuki Winarno:** Methodology, Validation, Resources, Writing—review & editing. **Budi Triyono:** Conceptualization, Supervision, Project administration, Writing—review & editing. **Yuli Prasetyo:** Methodology, Validation, Supervision, Writing—review & editing. **Suyitno Muslim:** Validation, Investigation, Formal analysis, Writing—review & editing.

Appendix A Reproducibility of Setting Calculations

The 21-row parameter table that drives Sections 3 and 4 is regenerated by the script `scripts/compute_setting.py` from the transformer and CT nameplate values listed in Table 2. The script writes `data/parameter_calc.csv` and prints a tabulated summary; all numbers reported in the manuscript can be traced to this CSV. The calculation flow follows the equations of Section 3 verbatim:

1. Nominal currents from $S/(\sqrt{3}\,U)$.
2. Rating currents at 110 % nominal.
3. Secondary CT currents at full load.
4. CT mismatch using (7).
5. Differential and restraint currents from (1).
6. Slope 1, Slope 2, and final setting current including the 0.30 A PLN headroom.

The 6 figures of the manuscript are produced by `scripts/generate_figures.py`, which writes both PDF (vector, included by LaTeX) and PNG (preview) versions to `figures/`. A clean rebuild on a Python 3.10+ environment with `numpy`, `matplotlib`, and `pandas` installed takes under 5 s on a commodity laptop.

The ETAP project files and the laboratory-trainer photos referenced in Sections 4 and 5 are excluded from the public repository to comply with personal-data protection rules of the underlying undergraduate project. They are available from the corresponding author for verification on request.

References

[1] IEEE Power Engineering Society: IEEE Guide for Protective Relay Applications to Power Transformers. IEEE Std C37.91-2021 (2021). https://doi.org/10.1109/IEEESTD.2021.9528404

[2] International Electrotechnical Commission: IEC 60076-1: Power transformers — Part 1: General. IEC Standard (2011)

[3] Ziegler, G.: Numerical Differential Protection: Principles and Applications, 2nd edn. Publicis Publishing, Erlangen, Germany (2012)

[4] Tripathy, M., Maheshwari, R.P., Verma, H.K.: Power transformer differential protection based on optimal probabilistic neural network. IEEE Transactions on Power Delivery **25**(1), 102–112 (2010) https://doi.org/10.1109/TPWRD.2009.2028800

[5] Hamilton, R.: Analysis of transformer inrush current and comparison of harmonic restraint methods in transformer protection. IEEE Transactions on Industry Applications **49**(4), 1890–1899 (2013) https://doi.org/10.1109/TIA.2013.2257155

[6] IEEE Power and Energy Society: IEEE Guide for the Application of Current Transformers Used for Protective Relaying Purposes. IEEE Std C37.110-2007 (2008). https://doi.org/10.1109/IEEESTD.2008.4534870

[7] Kang, Y.C., Lim, U.J., Kang, S.H., Crossley, P.A.: Compensation of the distortion in the secondary current caused by saturation and remanence in a CT. IEEE Transactions on Power Delivery **19**(4), 1642–1649 (2004) https://doi.org/10.1109/TPWRD.2004.835267

[8] Atiyah, W.A., Karimi, S., Moradi, M.: Transformer differential protection method for recognition between power transformer internal defects and inrush current: A comprehensive review of detection techniques. Applied Science and Engineering Progress (2024) https://doi.org/10.14416/j.asep.2024.07.008

[9] Siemens AG: SIPROTEC 7UT512 Differential Protection Relay — Manual. Order No. C53000-G1176-C107-1 (2010)

[10] Subari, M.A., Kusumastuti, S.: Analisis setting relay diferensial pada transformator daya. In: Proc. National Seminar on Electrical Engineering (2019). Author/year approximate; cited in source TA without full metadata

[11] Utomo, D.: Studi proteksi diferensial pada trafo tenaga di gardu induk. Jurnal Energi dan Kelistrikan **13**(2), 88–95 (2021). Cited in source TA; author/page numbers TBC

[12] Setiawan, A.P., Pratama, B.: Comparative study of differential protection setting on 30 mva transformer at pln substation using etap simulation. Journal on Advanced Research in Electrical Engineering (JAREE) **7**(1), 12–20 (2023). DOI verification pending; target journal candidate

[13] Zhang, J., Li, Y., Chen, X.: A review of differential protection schemes for modern power transformers: principles, implementation, and recent advances. Energies **15**(21), 8023 (2022) https://doi.org/10.3390/en15218023

[14] Bkhaitawi, A.H.Z., Abdoos, A.A., Ebadi, A.: Presenting an adaptive restraint method to improve performance of ground differential protection of power transformer. International Journal of Engineering **35**(11), 2213–2219 (2022) https:

//doi.org/10.5829/ije.2022.35.11b.16

[15] Chothani, N., Kumar, S.: Dynamic differential protection of transformer considering CT saturation based on waveform distortion estimation. IEEE Access **13**, 163832–163843 (2025) https://doi.org/10.1109/ACCESS.2025.3609541

[16] Tanha, M.H., Gandomkar, M., Nikoukar, J.: Coordination of protection and operation in micro-grids with inverter based distributed generation using SAOA. PLOS ONE **19**(10), 0311584 (2024) https://doi.org/10.1371/journal.pone.0311584

[17] Li, H., Wang, H.: Multi-objective optimization of relay protection setting based on MOAHA algorithm. Journal of Physics: Conference Series **2427**(1), 012043 (2023) https://doi.org/10.1088/1742-6596/2427/1/012043

[18] Gupta, P.K., Niranjan, P., Choudhary, N.K., Singh, N., Singh, R.K.: A novel multi-objective protection coordination scheme for a microgrid with optimal deployment of dual-setting ROCOV based relays. Protection and Control of Modern Power Systems **9**(4), 23–38 (2024) https://doi.org/10.23919/PCMP.2023.000425

[19] Kurniawan, Y., Handajadi, W.: Analisis sistem proteksi pada transformator daya 60 mva. Jurnal Elektro **9**(1), 12–19 (2017)

[20] Hatziargyriou, N., Milanović, J.V., Rahmann, C., Ajjarapu, V., Cañizares, C., Erlich, I., Hill, D., Hiskens, I., Kamwa, I., Pal, B., Pourbeik, P., Sanchez-Gasca, J., Stanković, A., Van Cutsem, T., Vittal, V., Vournas, C.: Definition and classification of power system stability — revisited & extended. IEEE Transactions on Power Systems **36**(4), 3271–3281 (2021) https://doi.org/10.1109/TPWRS.2020.3041774

[21] IEEE Standards Coordinating Committee 21: IEEE Standard for Interconnection and Interoperability of Distributed Energy Resources with Associated Electric Power Systems Interfaces. IEEE Std 1547-2018 (2018). https://doi.org/10.1109/IEEESTD.2018.8332112

[22] Ouyang, J., Tao, R., Xu, S., Yang, B.: Short-circuit calculation and adaptive distance protection for high penetration photovoltaic distribution network. Electric Power Systems Research **240**, 111281 (2025) https://doi.org/10.1016/j.epsr.2024.111281

[23] Muhammadia, K.B., Jufri, F.H., Husnayain, F.: Estimating rooftop photovoltaic penetration level on power distribution network constrained by power quality: Case study in salodong feeder. Journal of Advanced Technology and Multidiscipline **4**(1), 22–33 (2025) https://doi.org/10.20473/jatm.v4i1.71674

[24] Purba, D.A., Gani, U.A., Danial, D.: Study of Siemens 7UT86 percentage differential relay as protection of 60 MVA power transformer at 150 kv GIS dayeuh kolot. Telecommunications, Computers, and Electricals Engineering Journal **2**(2), 208–223 (2024) https://doi.org/10.26418/telectrical.v2i2.84598

[25] Thurner, L., Scheidler, A., Schäfer, F., Menke, J.-H., Dollichon, J., Meier, F., Meinecke, S., Braun, M.: pandapower—an open-source Python tool for convenient modeling, analysis, and optimization of electric power systems. IEEE Transactions on Power Systems **33**(6), 6510–6521 (2018) https://doi.org/10.1109/TPWRS.2018.2829021